

Simultaneous effects of polymer concentration, jet-stretching, and hot-drawing on microstructural development of wet-spun poly(acrylonitrile) fibers

Shahram Arbab · Parviz Noorpanah ·
Naser Mohammadi · Ahmad Zeinolebadi

Received: 9 April 2010 / Revised: 23 August 2010 / Accepted: 8 December 2010 /
Published online: 28 December 2010
© Springer-Verlag 2010

Abstract Investigation of structural development of acrylic fibers during the early stages of the wet-spinning process has great importance both in carbon fiber and textile industries. The simultaneous effects of increasing polymer concentration, jet-stretching and hot-drawing on porosity, morphology, and mechanical properties of wet-spun poly(acrylonitrile) fibers were studied. The detailed microstructure of the voids was characterized by electron microscopy, porosimetry, and thermoporometry. The effects of jet-stretching/hot-drawing on the overall porosity of the fibers were negligible below a threshold polymer concentration. Increasing polymer concentration from 10 to 20 vol.% reduced the total porosity. Hot-drawing was more effective in reducing the overall porosity of the fibers in comparison with jet-stretching. Stretching and drawing replaced the macrovoids by dense ligaments but did not change the volume fraction of nanovoids, however, shifted nanovoids size distribution toward smaller values. In general, Young's modulus and elongation at break increased by decreasing overall porosity, however, they depended also on the

S. Arbab

Engineering Faculty, Department of Textile Engineering, Guilan University, P.O. Box 41635-3756, Rasht, Iran

S. Arbab (✉) · P. Noorpanah

Textile Engineering Department, Amirkabir University of Technology, P.O. Box 15875-4413, Tehran, Iran

e-mail: a7928949@aut.ac.ir

N. Mohammadi

Polymer Engineering Department, Amirkabir University of Technology, P.O. Box 15875-4413, Tehran, Iran

A. Zeinolebadi

Institute of Technical and Macromolecular Chemistry, Department of Chemistry, University of Hamburg, Bundesstr. 45, 20146 Hamburg, Germany

distribution of voids size and chain orientation along the fiber axis. Strength-diameter correlation showed a good agreement with the Griffith's theory.

Keywords Wet-spinning · PAN fiber · Structure–property-relationship · Thermoporometry · Porosity

Introduction

In recent years, there has been an increasing demand for acrylic fibers due to their extensive application as the main precursor for high strength carbon fibers [1]. The properties of carbon fibers are strongly affected by the structure and physical properties of the precursor fibers [2, 3]. The acrylic fibers used in carbon fiber industry are mainly produced by wet-spinning process [4]. Wet-spinning is an interesting example of immersion precipitation and includes phase-separation and various transport phenomena [4–6]. As soon as the viscose polymeric solution is extruded into the coagulation bath, phase-separation begins due to solvent/non-solvent exchange and polymer chains precipitate as porous fibrils [4–7]. The structure of the porous fibrils is controlled by the rate and kinetics of phase-separation and gellation [4–7]. The as-spun fibers contain numerous macro and nanovoids [8]. The total porosity and the size of the voids determine drawability of the fiber in the next hot-drawing steps [8]. In addition, it has been shown that the structural defects such as voids and surface cracks of the precursor fibers are the main cause of fracture in carbon fibers [9]. Therefore, characterizing the porous structure of as-spun fibers in the early stages of the wet-spinning process and understanding the mechanisms of void healing are of great importance.

There are two main methods to control the size of the voids and reduce overall porosity of polymeric fibers in the wet-spinning process; namely preventing voids growth in the first steps of spinning and healing the previously formed voids by hot-drawing the as-spun fibers [10–13]. The former is usually achieved by variation of the spinning conditions such as dope composition and concentration [4–7], composition and temperature of the coagulation bath [4–7], and jet-stretching [11–13] while the latter is done by drawing the fibers in a hot water bath or hot steam (air) chambers [10]. For example, Frommer and Messalam [14] observed elimination of macrovoids in the final structure of the precipitated membrane by increasing polymer concentration from 7 to 30% in a system containing water, dimethyl sulfoxide, and cellulose acetate. Generally, increasing polymer concentration in the spinning dope leads to an increase in the viscosity. However, the rate of solvent/nonsolvent exchange and the rate of nucleation and growth of the voids decrease as a result of viscosity enhancement [10]. Won et al. [15] also observed low dope viscosity resulted in formation of macrovoids while high dope viscosity caused a significant reduction in the size and number of macrovoids. They attributed this effect to gelation of the polymeric phase, reduction in phase-separation rate, and inhibition of voids growth [15]. Van de Witte et al. [16] attributed the reduction of macrovoids to the enhancement of phase-separation delay time as a result of

increasing solution concentration. The reduction of macrovoids of wet-spun fibers by increasing jet-stretching ratio in the coagulation bath has been reported [17].

Sawai et al. [18, 19] showed the dependence of the final properties of ultrahigh-molecular-weight PAN fibers on draw ratio. They reported that orientation of polymer chains, density, and modulus increased with increasing draw ratio and reached a plateau at high draw ratios. Gupta et al. [12, 13] showed that drawing and its conditions had significant effects on the morphology of acrylic fibers.

In our previous article [8, 10, 20], we discussed thermodynamic aspects of wet-spinning process of acrylic fibers and applied thermoporometry as a strong method to characterize microstructure of voids. In this article, the simultaneous effects of polymer concentration, jet-stretching, and hot-drawing on the porosity development and the final properties of wet-spun PAN fibers were studied. Morphology of the fibers was investigated by scanning electron microscopy and the details of porosity (the size and size distribution of the voids) were further characterized by thermoporometry. The fraction of dense polymer ligament, macrovoids, and nanovoids were then calculated using porosimetry and thermoporometry data along with analysis of SEM micrographs.

Experimental

Materials

Poly(acrylonitrile-ran-methylacrylate) (94 wt% of acrylonitrile monomer) was provided by Polyacryl Co. (Isfahan, Iran). Dimethylformamide (DMF, Merck Ltd.) and tap-water were used as solvent and non-solvent, respectively. Viscosity average molecular weight, M_v , of the acrylic copolymer was measured by dilute solution viscometry of PAN/DMF solutions at 30 °C. Number average molecular weight, M_n , weight average molecular weight, M_w , and molecular weight distribution, PDI, was measured by gel permeation chromatography (GPC 150 C, Waters) at 30 °C in DMF. The columns of GPC apparatus were calibrated by polystyrene standard samples and DMF. The solvent was injected into five columns with a flow rate of 0.5 mL/min. The detection type was modular differential refractive index and values of $M_n = 36,000$ g/mol, $M_v = 70,000$ g/mol, $M_w = 116,000$ g/mol, and PDI = 3.2 were obtained. The obtained values agreed well with the values provided by the supplier.

Fiber spinning

Polymer powder was swelled in DMF for 24 h at 40 °C and was then mixed to homogeneous solutions with 10 to 20 vol.% of polymer. The prepared dope was then extruded by a metering pump (pump constant = 0.5 cm³/rev.) through a single-hole spinneret (diameter = 200 μm and $L/D = 1$) into a 1-m-long coagulation bath containing 50 wt% water and 50 wt% DMF at room temperature. The precipitated filament was wound on a bobbin with different draw ratios. The as-spun fibers were then hot-drawn in a bath containing hot water, 80 °C, and finally wound on a bobbin. Sample codes and spinning conditions are reported in Table 1.

Table 1 Dope polymer concentration and stretch/draw ratio

Sample code	Dope polymer concentration (vol.%)	Jet-stretch ratio	Hot-draw ratio
P10-F	10	1	—
P10-D4	10	4	—
P10-D2H2	10	2	2
P10-D1H4	10	1	4
P10-D2H4	10	2	4
P14-F	14	1	—
P14-D4	14	4	—
P14-D2H2	14	2	2
P14-D1H4	14	1	4
P14-D2H4	14	2	4
P20-F	20	1	—
P20-D4	20	4	—
P20-D2H2	20	2	2
P20-D1H4	20	1	4
P20-D2H4	20	2	4

Porosimetry

Overall porosity of fibers (dried for 24 h at ambient temperature) was assessed by measuring the weight and diameter of at least 50 one-meter-long specimens from randomly selected regions of wound fibers. Fiber diameter was determined by optical microscopy (Carl Ziess 533). The overall fiber porosity was calculated using the following equation [21, 22]:

$$\text{Overall porosity (\%)} = \frac{\pi R^2 L - m \rho_p^{-1}}{\pi R^2 L} \times 100 \quad (1)$$

where R , L , m , and ρ_p are radius, length, mass, and density of the sample, respectively.

Thermoporometry

Thermoporometry was conducted by differential scanning calorimetry (DSC) on water-saturated samples. Three to six milligrams of water saturated fibers were sealed and freezed in an aluminum pan at $-60\text{ }^\circ\text{C}$ and then heated with a rate of $1\text{ }^\circ\text{C}/\text{min}$ (DSC 2010, TA Instrument). For each sample, measurements were performed on four replicates and the representative data were reported.

Electron microscopy and image analysis

Fibers were freeze-fractured in liquid nitrogen. Fractured surface was then coated with a thin layer of gold and scanned with an electron microscope (Cambridge

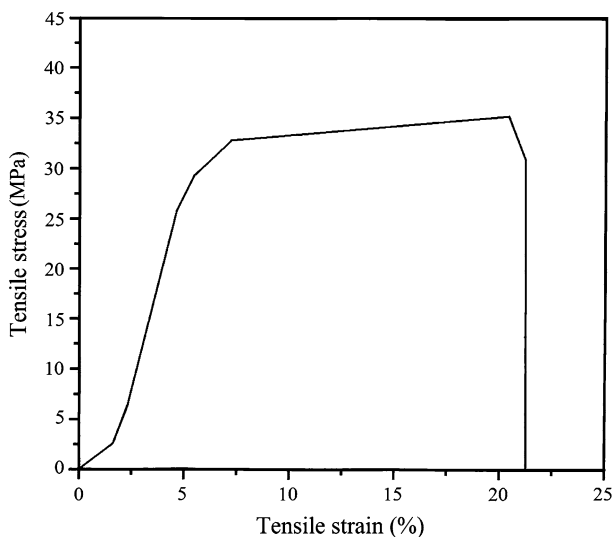


Fig. 1 Engineering stress–engineering strain of sample P20D1H4 in tensile test

ST360). The image analysis of SEM micrographs was conducted in Corel Draw[®] and MATLAB[®] software.

Tensile measurements

Single fiber mechanical properties (tensile strength, elastic modulus, and elongation at break) were obtained using an Instron tensile machine (model 5565) according to the ASTM D 3379-75 standard. Randomly selected fibers were centered and mounted straightly onto slotted paper frames with a 25 mm gauge length. The top and bottom ends of the fibers were fixed using a self-curing resin adhesive (Typax[®], Razi Co. Ltd.) and 24 h were led for the resin to harden at ambient temperature. The grip distance was set at 50 mm and the setup was then clamped on the tensile machine. Upon loading the mounted sample in the grips, the sides of the frame were cut gently with scissors. The sample was then stressed at a constant cross-head speed of 25 mm/min up to rupture. Figure 1 shows an engineering stress–engineering strain curve which is typical for all of the samples. Young's modulus was assessed by the slope of the curve (tangent method) below 1% strain. Only the results of the samples that were fractured from the middle portion were considered acceptable. For each sample type, the results of 15 acceptable replicates were averaged and reported.

Results and discussion

Figure 2 presents the overall porosity of all fibers with different spinning conditions and draw ratios. The reported porosity values have been averaged over 50 samples

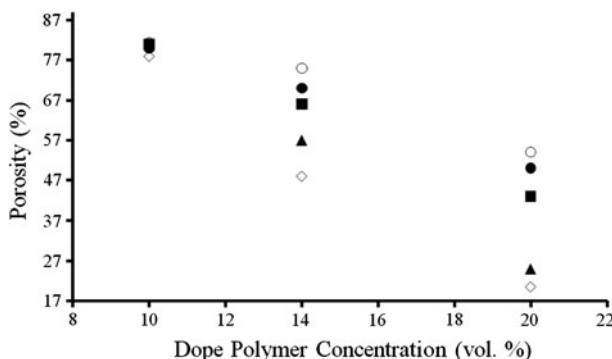


Fig. 2 Fibers' porosity percent versus dope polymer concentration: open circle Free, filled circle D4, filled triangle DIH4, filled square D2H2, open diamond D2H4. Sample codes are according to Table 1

(± 2 vol.%), thus the observed differences are real. Overall porosity was decreased by increasing polymer concentration, jet-stretching, or draw ratio. However, increasing jet-stretch or draw ratio had almost no effect on the overall porosity of the P10 series. This showed that there was a threshold concentration below which stretching and drawing were ineffective. In other words, the diffusion rate in this low concentration (viscosity) dope was so high that voids were formed in a short time and the overall porosity was too high to be removed by drawing. However, stretching and drawing affected the microstructure of P10 series fibers in a manner that will be discussed later. Further examination of Fig. 2 revealed that hot-drawing was more effective in reducing overall porosity than jet-stretching. For instance, the overall porosity of P14-D4 fiber was about 14 vol.% higher than P14-D1H4 fiber and the porosity of P20-D4 fiber was about 30 vol.% higher than P20-D1H4 fiber. This also indicated that the effect of drawing was enhanced at higher polymer concentrations. Indeed, increasing polymer concentration and draw ratio had synergistic effects in reducing the overall porosity.

The morphology of fibers with different spinning conditions and stretch/draw ratios are shown in Fig. 3 with different magnifications. All fibers had almost a circular cross-section, Fig. 3. It is worth mentioning that the circular cross-section is more preferred for manufacturing of carbon fibers than bean-like, oval, or doge-bone cross-sections [23]. All fibers possessed a dense center and finger-like channels in radial direction, Fig. 3. The dense center was enlarged by increasing polymer concentration. Indeed, by increasing polymer concentration, the gradient of solvent concentration between fiber and coagulation bath decreased while the resistance of fiber surface boundary increased due to the higher viscosity of solution. Thus, macrovoid formation was declined by increasing polymer concentration as a result of lower diffusion coefficients of solvent and non-solvent. The number, width, and length of the channels decreased when stretch/draw ratio increased. The SEM images also confirmed that hot-drawing was more effective in reducing the overall porosity than jet-stretching. For instance, in P20-D2H4 no macrovoids were detectable, Fig. 3c4. Indeed, jet-stretch and hot-drawing affect the porosity with different mechanisms. Hou et al. [24, 25] observed that diffusion coefficient of the

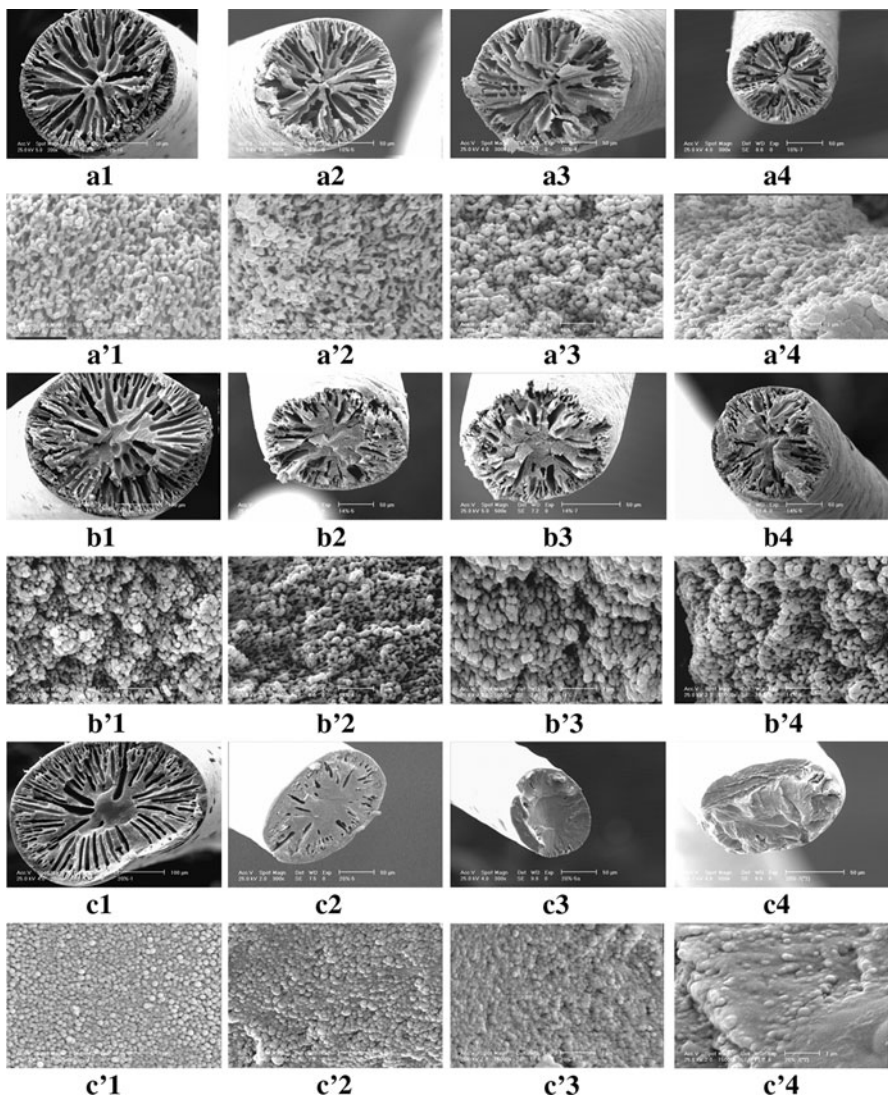


Fig. 3 SEM micrographs of fibers' cross-section; odd rows with lower magnification indicated by the scale bar and even rows with higher magnification (15,000 \times): **a1** & **a'1** (P10-F), **a2** & **a'2** (P10-D2H2), **a3** & **a'3** (P10-H4), **a4** & **a'4** (P10-D2H4), **b1** & **b'1** (P14-F), **b2** & **b'2** (P14-D2H2), **b3** & **b'3** (P14-H4), **b4** & **b'4** (P14-D2H4), **c1** & **c'1** (P20-F), **c2** & **c'2** (P20-D2H2), **c3** & **c'3** (P20-H4), **c4** & **c'4** (P20-D2H4)

solvent/non-solvent decreased in water/dimethyl sulfoxide/polyacrylonitrile and water/dimethyl formamide/polyacrylonitrile systems by increasing jet-stretching ratio. This effect has been attributed to the orientation of the voids along the fiber axis, increase of the dense ligament, and the loss of connectivity between voids (blocking transport channels of solvent and non-solvent) [10]. It is worth mentioning that the transport of solvent/non-solvent through channels is via fluid

flow, while the diffusion through dense ligament is via molecular diffusion which is much slower than the former [10]. In addition, increasing jet-stretch was achieved by increasing take-up speed of the fiber and reducing the residence time of the fibers in the coagulation bath. Therefore, imposing jet-stretch on the fibers reduced the growth rate of voids and also the available time for the growth. On the other hand, hot-drawing heals the previously formed voids due to the high mobility of polymer chains above their glass transition temperature which is about 60 °C [26] for polyacrylonitrile. The second mechanism seemed to be more effective than the first one in the same time scale. Figure 3 also presents the morphology of the fibers' cross-section with higher magnification (2nd, 4th, and 6th rows). It was seen that all fibers possessed a granular morphology. By increasing dope concentration, packing of granular domains was enhanced, whereas their size decreased. For instance, in P20-D2H4 fiber (Fig. 3c'4) the domains merged together and the surface of the fiber was smoother in comparison with P10-D2H4 (Fig. 3a'4) and P14-D2H4 (Fig. 3b'4) fibers. In addition, visual assessment of fibers showed that all samples' surfaces were milky white while P20-D2H4 sample was almost transparent and possessed a smooth surface.

The volume fractions of macrovoids (voids bigger than 1 μm), nanovoids (voids smaller than 1 μm), and dense ligament were calculated using image analysis of the SEM images and porosimetry data. The image analysis was conducted by Corel draw® and MATLAB® software. The difference between the overall porosity and the macrovoid fraction (assessed based on image analysis) gave the nanovoids fraction, Table 2.

By increasing dope concentration, the volume fraction of dense ligament increased. Interestingly, it is seen that in most cases drawing or stretching did not change the volume fraction of nanovoids significantly but the macrovoids were replaced by dense ligament. Therefore, it was concluded that the formation and volume fraction of nanovoids were thermodynamically controlled and were determined solely by phase-separation process. Nanovoids have been shown to increase the toughness of polymeric materials [27]. Therefore, survival of nanovoids through stretching/drawing process might be of great importance from a mechanical point of view.

The detailed characterization of the nanovoids was also conducted by thermoporometry. With this technique, the size distribution of the nanovoids was quantified by integrating the heat flow area of fusion of water (trapped in the nanovoids) that melted at temperatures below 0 °C. DSC heat flow curves, Fig. 4, were sliced to quantify the nanovoids cumulative percent according to the well-known theories [8, 28, 29].

The cumulative nanovoids' percent of P10, P14, and P20 series and their comparison have been shown in Fig. 5a–d. By comparing the three graphs, it was seen that the distribution of nanovoids shifted toward smaller sizes by increasing dope concentration at the same stretch/draw ratio. In addition, the size distribution shifted toward smaller sizes by imposing stretch or draw on the fibers. Although, stretching and drawing did not affect the total volume percent of the nanovoids, Table 2, but they reduced the size of the nanovoids. The smaller the nanovoids were, the more effective they were in toughening the fiber [27].

Table 2 Dense ligament, macrovoids, and nanovoids fractions in fibers

Stretch & draw ratio	P10 series			P14 series			P20 series		
	Dense ligament	Macrovoids (vol.%)	Nanovoids (vol.%)	Dense ligament (vol.%)	Macrovoids (vol.%)	Nanovoids (vol.%)	Dense ligament (vol.%)	Macrovoids (vol.%)	Nanovoids (vol.%)
Free	18.5	61	20.5	25	45	30	43	34	23
D4	18	62	20	30	38	32	50	24.5	25.5
D2H2	19	61	21	34	33	33	58	16	26
DIH4	19.5	60.5	20	45	27	32	70	5	25
D2H4	22	60	18	52	20	28	80	0	20

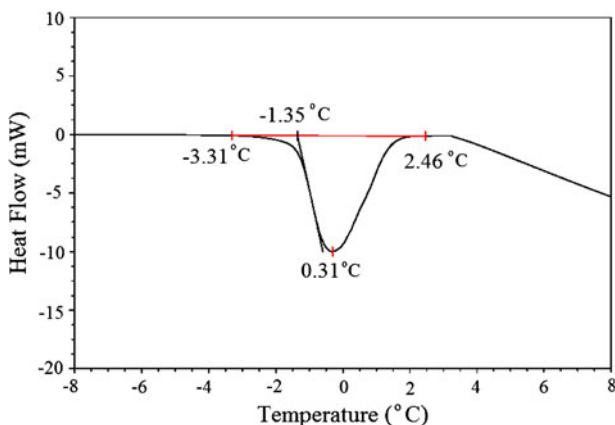


Fig. 4 Typical DSC heat flow curve of ice-melting in saturated porous fiber (P14-F)

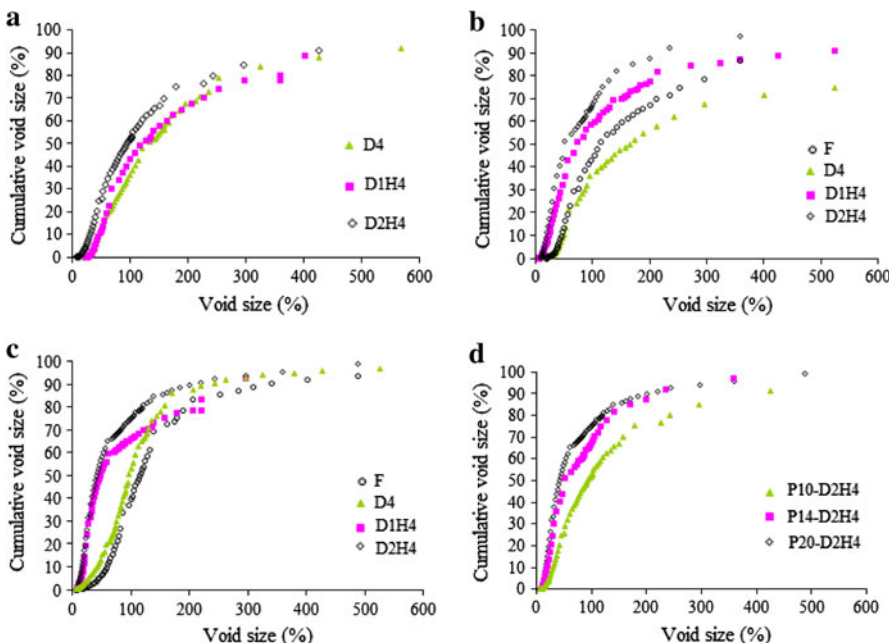


Fig. 5 Effect of jet-stretch and hot-draw ratio on the cumulative nanovoids distribution: **a** P10 series, **b** P14 series, **c** P20 series, **d** Comparison of D2H4 series

Young's modulus of all fibers has been shown in Fig. 6. Theoretically, modulus of porous materials shows an exponential dependence on the overall porosity [30]. Modulus was increased by decreasing the overall porosity of the fibers. However, all P10 series fibers possessed almost the same overall porosity but they had different moduli. This might be attributed to the different size of the nanovoids as revealed by thermoprometry curves, Fig. 5a. In addition, stretching and drawing increased the

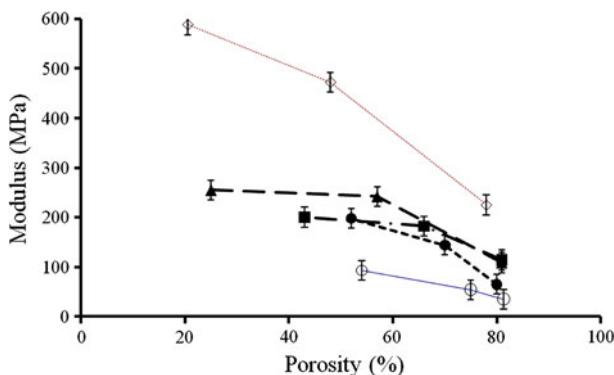


Fig. 6 Fibers' Young modulus versus fiber overall porosity *open circle* Free, *filled circle* D4, *filled triangle* D1H4, *filled square* D2H2, *open diamond* D2H4 (Lines are guide to the eye)

orientation of chains along the fiber axis. Chain orientation also has been shown to increase fiber modulus [18, 19, 31]. Although, overall porosity remained unchanged by stretching and drawing but the voids became smaller in size. Therefore, it can be concluded that modulus not only depends on the overall porosity but also depends on the size of the voids and also the degree of chain orientation.

Elongation at break was increased by decrease of the overall porosity, Fig. 7. The same trend as modulus was observed for P10 series. Voids are stress-concentration zones and initiate crazes when the sample is stressed. Thus, increase of the number or the size of voids resulted in fracture of the fibers at smaller strains.

In addition, stretching/drawing caused a reduction in the fiber diameter. According to the Girifffth's theory, the reciprocal of the strength, σ , is proportional to the square root of the diameter, D , [32]:

$$\sigma^{-1} \propto D^{0.5} \quad (2)$$

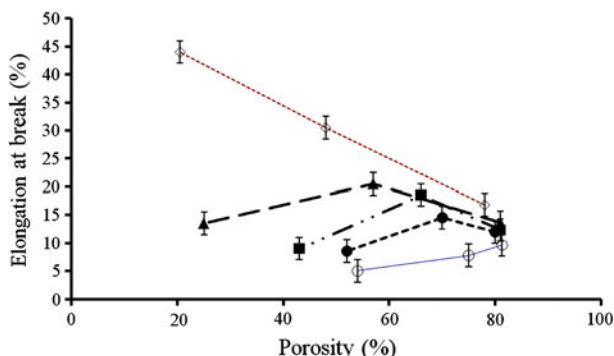


Fig. 7 Elongation at break versus overall porosity of the fibers: *open circle* Free, *filled circle* D4, *filled triangle* D1H4, *filled square* D2H2, *open diamond* D2H4 (Lines are guide to the eye)

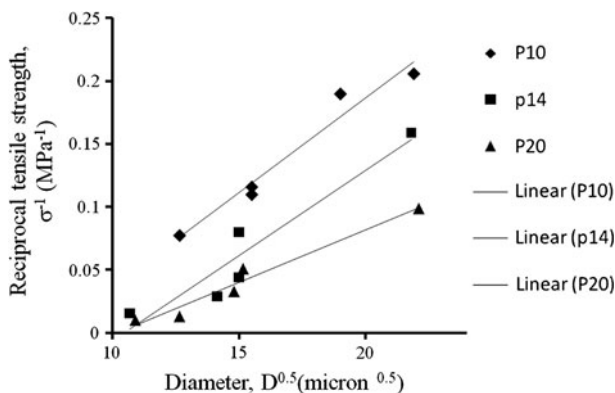


Fig. 8 Reciprocal strength versus second root of fibers' diameter (*Lines* are best linear regression)

we also, found the same correlation in our samples, Fig. 8. Thus, stretching/drawing led to higher mechanical properties through reduction in the overall porosity, void size, and fiber diameter.

Conclusions

The overall porosity of wet-spun PAN fibers decreased with increasing polymer concentration, jet-stretching, and hot-drawing. The effects of stretching and drawing on the overall porosity of the fibers were negligible under a threshold polymer concentration. In addition, hot-drawing was more effective in reducing the overall porosity of the fibers than jet-stretching. Jet-stretching and hot-drawing replaced macrovoids by dense ligament but did not change the volume fraction of nanovoids, however, shifted the size distribution of nanovoids toward smaller values. Fibers' modulus and elongation at break increased by decreasing the overall porosity. It was also seen that modulus not only depended on the overall porosity but also depended on the size of voids and orientation of the polymer chains along the fiber's axis. Finally, reciprocal of the strength was proportional to the square root of the diameter, agreeing well with the Griffith's theory.

References

1. Paiva MC, Katasthane P, Edie DD, Ogale AA (2003) UV stabilization route for melt-processible PAN-based carbon fibers. Carbon 41:1399–1409
2. Mittal J, Mathur RB, Bahl OP, Inagaki M (1998) Post spinning treatment of PAN fibers using succinic acid to produce high performance carbon fibers. Carbon 36:893–897
3. Thünenmann AF, Ruland W (2000) Microvoids in polyacrylonitrile fibers: a small-angle X-ray scattering study. Macromolecules 33:1848–1852
4. Salem DR (2001) Structure formation in polymeric fibers. Hanser, Munich

5. Chen J, Wang C, Dong X, Liu H (2006) Study on the coagulation mechanism of wet-spinning PAN fibers. *J Polym Res* 13:515–519
6. Wang YX, Wang CG, Yu MJ (2007) Effects of different coagulation conditions on polyacrylonitrile fibers wet spun in a system of dimethylsulphoxide and water. *J Appl Polym Sci* 104:3723–3729
7. Masson JC (1995) Acrylic fiber technology and application. Marcel Decker, New York
8. Arbab S, Noorpanah P, Mohammadi N, Soleimani M (2008) Designing index of void structure and tensile properties in wet-spun polyacrylonitrile (PAN) fiber. I. Effect of dope polymer or nonsolvent concentration. *J Appl Polym Sci* 109:3461–3469
9. Chen JC, Harrison IR (2002) Modification of polyacrylonitrile (PAN) carbon fiber precursor via post-spinning plasticization and stretching in dimethyl formamide (DMF). *Carbon* 40:25–45
10. Arbab S, Mohammadi N, Noorpanah P (2008) The synergistic effect of dope concentration and jet-drawing on structure development of wet-spun poly(acrylonitrile). *e-Polymers* 080
11. Bajaj P, Sreekumar TV, Sen K (2002) Structure development during dry-jet-wet spinning of acrylonitrile/vinyl acids and acrylonitrile/methyl acrylate copolymers. *J Appl Polym Sci* 86:773–787
12. Gupta B, Revagada N, Anjum N, Atthoff B, Hilborn J (2006) Preparation of poly(lactic acid) fiber by dry-jet-wet-spinning. I. Influence of draw ratio on fiber properties. *J Appl Polym Sci* 100:1239–1246
13. Gupta B, Revagada N, Anjum N, Atthoff B, Hilborn J (2006) Preparation of poly(lactic acid) fiber by dry-jet-wet spinning. II. Effect of process parameters on fiber properties. *J Appl Polym Sci* 101:3774–3780
14. Frommer MA, Messalam RM (1973) Mechanism of membrane formation. VI. Convective flows and large void formation during membrane precipitation. *Ind Eng Chem* 12:328–334
15. Won J, Park HC, Kim UY, Kang YS, Yoo SH, Jho JY (1999) The effect of dope solution characteristics on the membrane morphology and gas transport properties: PES/ γ -BL/NMP system. *J Membr Sci* 162:247–255
16. Van de Witte P, Dijkstra PJ, van den Berg JWA, Feijen J (1996) Phase separation processes in polymer solutions in relation to membrane formation. *J Membr Sci* 117:1–31
17. Mikolajczyk T, Bogun M, Blazewicz M, Piekarzky I (2006) Effect of spinning conditions on the structure and properties of PAN fibers containing nano-hydroxyapatite. *J Appl Polym Sci* 100:2881–2888
18. Sawai D, Kanamoto T, Yamazaki H, Hisatani K (2004) Dynamic mechanical relaxations in poly(acrylonitrile) with different stereoregularities. *Macromolecules* 37:2839–2846
19. Sawai D, Fujii Y, Kanamoto T (2006) Development of oriented morphology and tensile properties upon superdawing of solution-spun fibers of ultra-high molecular weight poly(acrylonitrile). *Polymer* 47:4445–4453
20. Arbab S, Mohammadi N, Noorpanah P (2008) Designing index of void structure and tensile modulus in wet-spun poly(acrylonitrile) proto-fibres. Part II: synergistic effect of dope non-solvent concentration and jet draw ratio. *Iran Polym J* 17:227–235
21. Chou WL, Yang MC (2005) Effect of take-up speed on physical properties and permeation performance of cellulose acetate hollow fiber. *J Membr Sci* 250:259–267
22. Fan SC, Wang Y, Li C, Lee K, Liaw D, Huang H, Lai JYJ (2002) Effect of coagulation media on membrane formation and vapor permeation performance of novel aromatic polyamide membrane. *J Membr Sci* 204:67–79
23. Radishevslia MB, Serkov AT, Budnitskii G, Medvedev VA, Zlatoustova LA (2005) Improvement of manufacturing technology for ultrastrong and high-modulus carbon fibres. *Fiber Chem* 37:327–331
24. Hou C, Qu R, Wang L, Ying L (2006) Diffusion coefficient of DMF in acrylic fiber formation. *J Appl Polym Sci* 101:3616–3619
25. Hou C, Liang Y, Wang CG (2005) Determination of the diffusion coefficient of H₂O in polyacrylonitrile fiber formation. *J Polym Res* 12:49–52
26. Bajaj P, Sreekumar TV, Sen K (2001) Thermal behaviour of acrylonitrile copolymers having methacrylic and itaconic acid comonomers. *Polymer* 42:1707–1718
27. Dutriez C, Satoh K, Kamigaito M, Yokoyama H (2007) Nanometer voids prevent crack growth in polymeric materials. *Macromolecules* 40:7433–7436
28. Wulff M (2004) Pore size determination by thermoporometry using acetonitrile. *Thermochim Acta* 419:291–294
29. Iza M, Woerly S, Danumah C, Kaliaguine S, Bousmina M (2000) Determination of pore size distribution for mesoporous materials and polymeric gels by means of DSC measurements: thermoporometry. *Polymer* 41:5885–5893

30. Sonnenschien MF (2003) Porosity-dependent Young's modulus of membranes from polyetherether ketone. *J Polym Sci Phys Ed* 41:1168–1174
31. Xu Q, Xu L, Cao W, Wu S (2005) A study on the orientation structure and mechanical properties of polyacrylonitrile precursors. *Polym Adv Technol* 16:642–645
32. Griffith AA (1921) The phenomena of rupture and flow in solids. *Philos Trans R Soc Lond Ser A* 221:163–198